

## *Ab initio* study of charge transfer in low-energy collisions of $\text{Si}^{4+}$ with helium

P. C. Stancil\* and B. Zygelman†

*W. M. Keck Laboratory for Computational Physics, Department of Physics, University of Nevada Las Vegas, Las Vegas, Nevada 89154-4002*

N. J. Clarke‡ and D. L. Cooper§

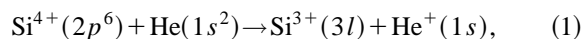
*Department of Chemistry, University of Liverpool, P. O. Box 147, Liverpool L69 3BX United Kingdom*  
(Received 21 June 1996)

We present state-dependent and total charge transfer cross sections for the process  $\text{Si}^{4+}(2p^6) + \text{He}(1s^2) \rightarrow \text{Si}^{3+}(3l) + \text{He}^+(1s)$ , where  $l = s, p$ , in the collision energy range 0.004–10 eV/amu. The cross sections are determined using a close-coupled quantal method. Fully *ab initio* adiabatic potentials and nonadiabatic radial coupling matrix elements obtained with the spin-coupled valence-bond method are incorporated. Rate coefficients for temperatures between 1000 and 50 000 K and results for isotopic  $^3\text{He}$  are also presented. Astrophysical applications are briefly discussed. [S1050-2947(97)00902-5]

PACS number(s): 34.70.+e, 31.30.Gs

### I. INTRODUCTION

Butler and Dalgarno [1] investigated the charge transfer recombination process



where  $l = s, p$ , using the Landau-Zener approximation and an empirical model of the potentials. Opradolce, McCarroll, and Valiron [2] solved the quantum-mechanical scattering equations for process (1) and calculated the  $\text{SiHe}^{4+}$  adiabatic energies using the model potential method, which can be optimized to give nearly exact asymptotic separated-atom energies. Opradolce *et al.* find the charge transfer rate coefficients to have a significant temperature dependence, while the results of Butler and Dalgarno are nearly temperature independent. The discrepancy was attributed to Butler and Dalgarno's empirical potentials and not to a failing of the Landau-Zener approximation.

We present an *ab initio* investigation of reaction (1) in which the scattering equations are solved through a fully quantum-mechanical, close-coupled, molecular-orbital approach [3]. We include only radial coupling since Opradolce *et al.* have shown that rotational coupling contributes negligibly below  $\sim 50$  eV. We discuss the spin-coupled valence-bond (SCVB) calculations in Sec. II. The charge transfer results and discussion are presented in Sec. III, while Sec. IV addresses astrophysical applications. All notation is in atomic units unless otherwise noted.

### II. ELECTRONIC STRUCTURE CALCULATIONS

Adiabatic potentials and radial coupling matrix elements were obtained using the SCVB approach. The basic strategy

is very similar to that described in a previous work [4] and so we indicate here only those features that are particularly salient to the present study. Further details can be found elsewhere [5].

We adopted Dunning correlation-consistent basis sets (triple- $\zeta$ -valence quality) for Si/He consisting of  $(15s9p2d/6s2p)$  Gaussian-type orbitals contracted to  $[5s4p2d/3s2p]$ . SCVB expansions were performed in the space of the two valence electrons, with the  $\text{Si}(1s^22s^22p^6)$  core described by (optimized) molecular orbitals taken from appropriate state-averaged, full-valence complete-active-space self-consistent-field calculations [5]. All single and double vertical excitations plus singly ionic cross excitations were included into three  $\sigma$ , two  $\pi$ , and one  $\delta$  virtual orbitals for each valence electron, generating very compact SCVB wave functions consisting of just 46 valence-band structures [5]. The calculations were carried out for 34 internuclear separations  $R$  from 1.8 to 14.

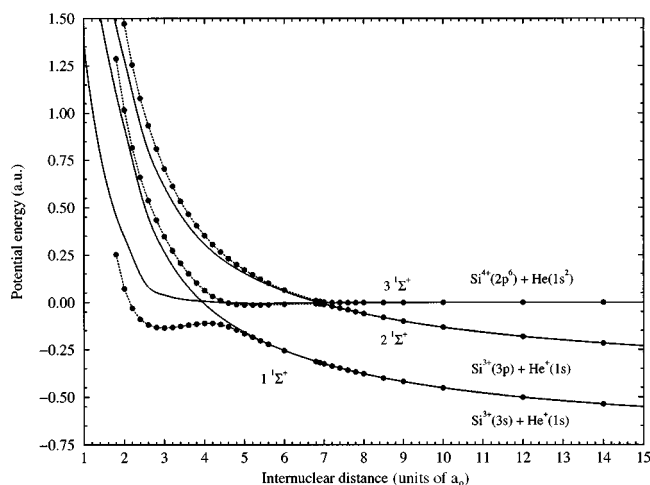


FIG. 1.  $1^1\Sigma^+$  adiabatic (dotted line) and diagonal diabatic (full line) potential energies for the  $\text{SiHe}^{4+}$  system as a function of internuclear distance  $R$ .

\*Electronic address: stancil@physics.unlv.edu

†Electronic address: bernard@physics.unlv.edu

‡Electronic address: nickc@tc.bham.ac.uk

§Electronic address: dlc@rs2.ch.liv.ac.uk

TABLE I. Asymptotic separated-atom energies for the three lowest  $1\Sigma^+$  states of  $\text{SiHe}^{4+}$ .

Molecular state	Asymptotic atomic states	Energy (eV)	
		Theory	Expt. <sup>a</sup>
$1\Sigma^+$	$\text{Si}^{3+}(3s^2S) + \text{He}^+(1s)$	-20.438	-20.550
$2\Sigma^+$	$\text{Si}^{3+}(3p^2P) + \text{He}^+(1s)$	-11.705	-11.709
$3\Sigma^+$	$\text{Si}^{4+}(2p^6^1S) + \text{He}(1s^2)$	0.0	0.0

<sup>a</sup>Reference [6].

The resulting adiabatic potential energies are displayed in Fig. 1. Visual inspection suggests close agreement with Opradolce *et al.* [2], but, since numerical data are not available in Ref. [2], quantitative comparison is not possible. The SCVB approach is a fully flexible *ab initio* technique that can describe close nuclear separations, i.e., the molecular region, with much the same accuracy as the asymptotic limits. On the other hand, the model potential method of Opradolce *et al.* [2] incorporates adjustable parameters that enable the potentials to reproduce exactly the separated-atom behavior, but they may not describe the molecular region with comparable accuracy. Table I presents the calculated and experimental separated-atom energies relative to the neutral incoming channel. The agreement is excellent, with a maximum difference of only 0.55% for the non-dominant  $3s$  channel. We did not calculate any higher-lying  $1\Sigma^+$  states, the next three of which correlate to  $\text{Si}^{3+}(3d) + \text{He}^+(1s)$ ,  $\text{Si}^{2+}(3s^2) + \text{He}^{2+}$ , and  $\text{Si}^{3+}(4s) + \text{He}^+(1s)$ , respectively. The first has an avoided crossing near  $R_* = 120$ , while the latter two are endothermic by 0.37 and 3.5 eV, respectively. For the low-energy regime considered in the present calculations, their contribution to the total cross sections and rate coefficients is likely to be negligible.

The avoided crossing distances  $R_*$  and the corresponding energy gaps  $\Delta U(R_*)$  are listed in Table II for the empirical potentials of Butler and Dalgarno [1], the model potentials of Opradolce *et al.* [2], and the present SCVB potentials. Whereas the positions of the avoided crossings are in close agreement, the three methods predict significantly different values for  $\Delta U(R_*)$  with the SCVB result always the largest. For both crossings, the SCVB method gives values of  $\Delta U(R_*)$  that are  $\sim 40\%$  larger than those of Opradolce *et al.* [2].

We currently have no absolute criterion for assigning phases to the peaks of the radial couplings. Phase changes were imposed when matrix elements otherwise approached

TABLE II. Avoided crossings and adiabatic potential differences at avoiding crossings for the  $1\Sigma^+$  states of  $\text{SiHe}^{4+}$ .

Molecular state	Asymptotic atomic states	$R_*$ ( $a_0$ )		
		Ref. [1]	Ref. [2]	This work
$1\Sigma^+$	$\text{Si}^{3+}(3s^2S) + \text{He}^+$	4.0	4.5	4.6
		2.1	2.46	3.385
$2\Sigma^+$	$\text{Si}^{3+}(3p^2P) + \text{He}^+$	7.0	6.975	7.0
		0.112	0.244	0.344

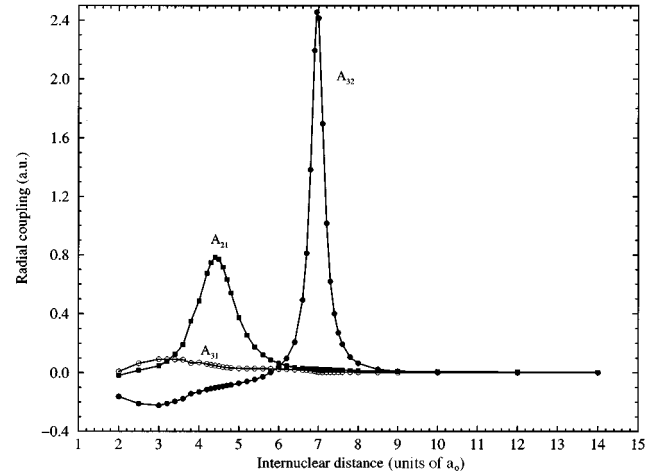


FIG. 2.  $1\Sigma^+$  nonadiabatic radial couplings for the  $\text{SiHe}^{4+}$  system as a function of internuclear distance  $R$ .

zero with a gradient sufficient to introduce discontinuities. The calculated radial couplings (matrix elements of  $\partial/\partial R$ ) are illustrated in Fig. 2. The peaks corresponding to the two avoided crossings are smooth, well defined, and centered directly on the positions of the crossings. The significant coupling evident in  $A_{32}$  for  $R \leq 5$  is a consequence of the existence of two noninteracting avoided crossings and a molecular-orbital approach [7]. A pure Lorentzian behavior is characteristic of the atomic-orbital approximation. As is intuitively reasonable, the couplings between nonadjacent states are much smaller than those between adjacent states. Comparisons cannot be made with previous work because Opradolce *et al.* [2] give no information on the radial couplings they used.

### III. RESULTS AND DISCUSSION

The charge transfer cross sections are obtained in the present calculation by a fully quantum-mechanical, close-coupling, molecular-orbital method. The method has been fully described elsewhere [3]. The calculations are performed in the diabatic representation. The diagonal elements of di-

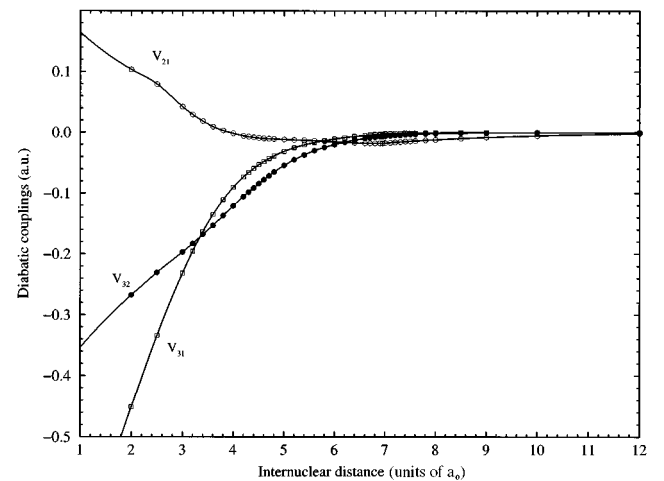


FIG. 3.  $1\Sigma^+$  off-diagonal diabatic potentials for the  $\text{SiHe}^{4+}$  system as a function of internuclear distance  $R$ .

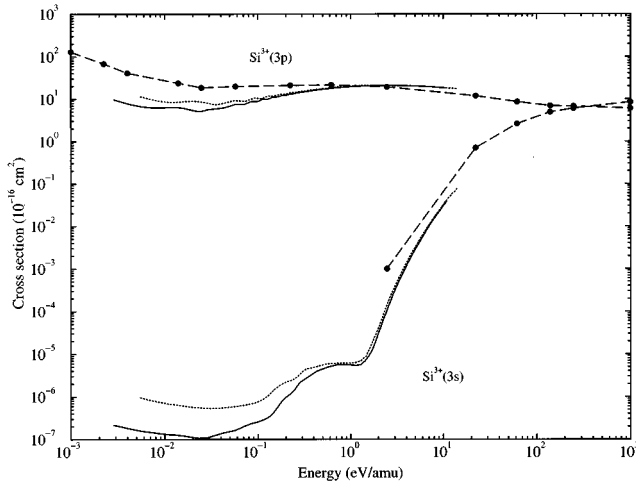


FIG. 4. State-dependent electron capture cross sections.  $\text{Si}^{4+} + {}^4\text{He}$ , this work (full lines) and Ref. [2] (dashed lines),  $\text{Si}^{4+} + {}^3\text{He}$ , this work (dotted lines). The center-of-mass collision energy  $E$  has been divided by the nuclear reduced mass  $\mu$ .

adiatic potential matrix are given in Fig. 1, whereas the off-diagonal elements are displayed in Fig. 3.

State-dependent and total charge transfer cross sections for process (1) are presented in Figs. 4 and 5, respectively, as a function of the center-of-mass collision energy  $E$  divided by the nuclear reduced mass  $\mu$ . Electron capture into the  $3p$  state is the dominant channel throughout the whole energy range of this study. Not until the collision energy is  $\geq 25$  eV/amu does capture into the  $3s$  state begin to contribute significantly. The present cross sections are in qualitative agreement with the calculations of Opradolce *et al.* [2], though the current  $3s$  results are typically a factor of 5 smaller, while the  $3p$  (and total) results are greater for energies  $\geq 2$  eV/amu and smaller for energies  $\leq 2$  eV/amu. This discrepancy cannot be attributed to the neglect of rotational coupling or electron translation factors since Opradolce *et al.* have shown the two effects are negligible in this system for energies  $\leq 15$  and 150 eV/amu, respectively. A two-channel Landau-Zener analysis using the  $R_*$  and  $\Delta U(R_*)$  data from

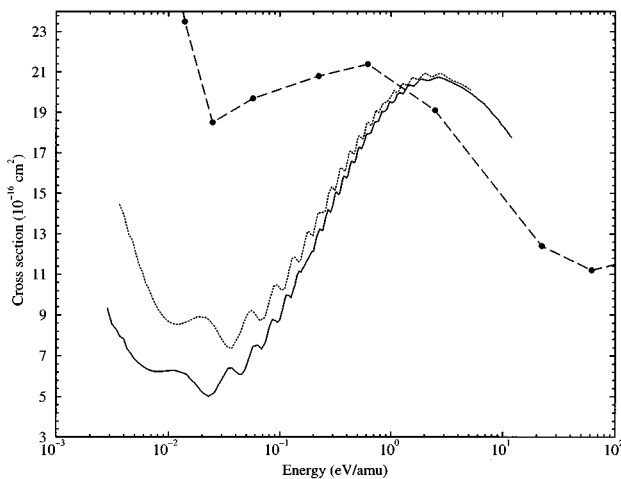


FIG. 5. Total electron capture cross sections. The designations are as given in Fig. 4.

Table II can qualitatively reproduce this trend suggesting that the cross sections are sensitive to the adiabatic potential difference at the avoided crossing. While it can be argued that the model potential method will be reliable for predicting  $R_*$  since the asymptotic separated-atom energies are fit exactly to experimental values, the same cannot be said of  $\Delta U(R_*)$ . An *ab initio* technique is necessary to describe the molecular region and hence obtain an accurate value of  $\Delta U(R_*)$ . Merged-beams measurements of the low-energy cross sections would be useful to discriminate between the two theoretical approaches.

Stancil and Zygelman [8] have discussed the influence of a kinematic isotope effect on the total charge transfer cross section at low energy. They gave the simple formula, derived from the Landau-Zener approximation, to relate the  ${}^4\text{He}$  target cross section to the  ${}^3\text{He}$  target

$$\frac{\sigma({}^3\text{He})}{\sigma({}^4\text{He})} \approx \frac{1 - 2V_{11}(R_*)/[\mu({}^3\text{He})v^2]}{1 - 2V_{11}(R_*)/[\mu({}^4\text{He})v^2]}, \quad (2)$$

where  $V_{11}$  is the diabatic potential for the entrance channel and  $v$  the relative collision velocity. For  $\text{Si}^{4+} + \text{He}$ , Eq. (2) predicts a threshold for the isotope effect, the  ${}^3\text{He}$  target cross section 2% larger than the  ${}^4\text{He}$  target cross section, of  $\sim 0.5$  eV/amu and  $\sigma({}^3\text{He})/\sigma({}^4\text{He}) \sim 1.1$  at 0.1 eV/amu. The quantum calculation gives a threshold of  $\sim 1$  eV/amu and  $\sigma({}^3\text{He})/\sigma({}^4\text{He}) \sim 1.16$  at 0.1 eV/amu, verifying the predictions of Eq. (2). Cross sections for  ${}^3\text{He}$  targets are presented in Figs. 4 and 5.

Figure 6 presents partial cross sections  $\sigma_J$  versus angular momentum  $J$  for capture into  $\text{Si}^{3+}(3p)$  from collisions of  $\text{Si}^{4+}$  with both  ${}^4\text{He}$  and  ${}^3\text{He}$  targets at small and large collision energies. The origin of the enhanced  ${}^3\text{He}$  cross section at low collision energies is apparent from Fig. 6(a), where the maximum partial cross section for  ${}^3\text{He}$   $\sigma_{J=25}$  is more than twice as large as  $\sigma_{J=30}$ , the maximum partial cross

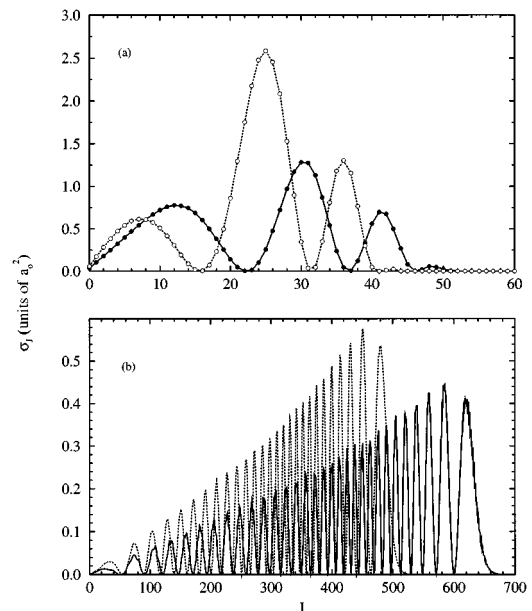


FIG. 6. Partial cross sections  $\sigma_J$  versus  $J$  for capture into  $\text{Si}^{3+}(3p)$  from  $\text{Si}^{4+} + {}^4\text{He}$  (full lines) and  $\text{Si}^{4+} + {}^3\text{He}$  (dotted lines). (a)  $E=0.01$  eV/amu and (b)  $E=5$  eV/amu.

section for  ${}^4\text{He}$ . The angular momentum of the global (and local) peak partial cross sections are shown numerically in Fig. 6(a) to be related through the equation

$$J_4(J_4+1) \sim \frac{\mu({}^4\text{He})}{\mu({}^3\text{He})} J_3(J_3+1), \quad (3)$$

where  $J_4$  ( $J_3$ ) is the angular momentum with  ${}^4\text{He}$  ( ${}^3\text{He}$ ) targets. An analogous expression can be obtained classically from the relations  $b = \sqrt{J(J+1)}/\mu v$  and  $b^{\max} \approx R_* \sqrt{1 - 2V_{11}(R_*)/\mu v^2}$  where  $b^{\max}$  is the maximum impact parameter for which a trajectory can enter the reaction region and charge transfer. It is interesting to note that the  $b$  ( $J$ ) of the local partial cross section peaks have the same mass dependence as  $b^{\max}$  ( $J^{\max}$ ). Equation (3) also implies  $b_4 \sim \sqrt{\mu({}^3\text{He})/\mu({}^4\text{He})} b_3$ , the so-called focusing effect. For large collision energies, while the  ${}^3\text{He}$  partial cross sections are larger than for  ${}^4\text{He}$ , as shown in Fig. 6(b), the  ${}^4\text{He}$  partial cross sections remain significant to much higher  $J$ , resulting in nearly identical total cross sections regardless of target mass. For large  $J$  (and large energy), Eq. (3) is replaced by  $J_4 \sim \mu({}^4\text{He})/\mu({}^3\text{He}) J_3$  and the impact parameter becomes target-mass-independent.

Unlike earlier investigations, the current calculations consist of an energy grid of typically 25 points per decade revealing features previously hidden. Superimposed over a monotonic behavior, the total cross sections display a pronounced oscillatory structure, which may be interpreted as a type of Stueckelberg oscillation [9,10,3]. The number of oscillations

TABLE III. State-dependent rate coefficients  $\alpha$  ( $\text{cm}^3 \text{ s}^{-1}$ ) as a function of temperature  $T$ . Fitting parameters  $a_i$  ( $\text{cm}^3 \text{ s}^{-1}$ ),  $b_i$ , and  $c_i$  (K) according to Eq. (4) are given at the end of the table. The numbers in brackets denote multiplicative powers of ten.

$T$ (K)	${}^4\text{He}$		${}^3\text{He}$	
	$3s$	$3p$	$3s$	$3p$
1000	4.14[-18]	1.68[-10]	1.97[-17]	2.57[-10]
2000	1.33[-17]	3.02[-10]	5.21[-17]	4.32[-10]
3000	3.28[-17]	4.34[-10]	9.89[-17]	5.97[-10]
4000	6.04[-17]	5.60[-10]	1.51[-16]	7.52[-10]
5000	9.26[-17]	6.80[-10]	2.03[-16]	8.96[-10]
6000	1.27[-16]	7.94[-10]	2.54[-16]	1.03[-9]
7000	1.62[-16]	9.02[-10]	3.09[-16]	1.16[-9]
8000	1.98[-16]	1.01[-9]	3.74[-16]	1.28[-9]
9000	2.35[-16]	1.10[-9]	4.62[-16]	1.39[-9]
10000	2.77[-16]	1.19[-9]	5.89[-16]	1.50[-9]
15000	7.46[-16]	1.62[-9]	2.69[-15]	1.98[-9]
20000	2.56[-15]	1.97[-9]	1.04[-14]	2.37[-9]
30000	1.81[-14]	2.64[-9]	6.53[-14]	3.01[-9]
40000	6.67[-14]	3.03[-9]	2.15[-13]	3.52[-9]
50000	1.67[-13]	3.42[-9]	4.97[-13]	3.93[-9]
$a_1$	5.51[-16]	1.31[-9]	1.00[-15]	1.64[-9]
$b_1$	2.14	8.90[-1]	1.70	8.07[-1]
$c_1$	1.37+4	1.00[+5]	9.07[+3]	1.09[+5]
$a_2$	5.23[-17]		4.29[-16]	
$b_2$	7.41		6.00	
$c_2$	1.29[+4]		1.94[+4]	

is slightly larger for the heavier  ${}^4\text{He}$  target as was noted for the  $\text{N}^{4+} + \text{H(D)}$  charge-transfer system [8]. These types of features have yet to be experimentally confirmed for low-energy multiply charged systems and it appears likely to remain so due to the required energy resolution and cross-section sensitivity.

Rate coefficients for reaction (1) have been determined by averaging the cross section over a Maxwellian velocity distribution. State- and target-isotope-dependent rate coefficients are presented in Table III. Figure 7 displays the total rate coefficients in comparison to previous calculations. The rates are fit to the parametric form

$$\alpha(T) = \sum_i a_i \left( \frac{T}{10000} \right)^{b_i} \exp\left( \frac{-T}{c_i} \right), \quad (4)$$

with the parameters  $a_i$  ( $\text{cm}^3 \text{ s}^{-1}$ ),  $b_i$ , and  $c_i$  (K) given in Table III. The fits are reliable to within 5% and 15% for capture into the  $3p$  and  $3s$  channels, respectively, over the determined temperature range. The current results have a stronger temperature dependence than any of the previous investigations. The discrepancies increase with decreasing temperature. For  $T=1000$  K, our rate coefficient is a factor of 2.9 smaller than the value determined by Opradolce *et al.* [2]. A direct measurement of the rate coefficient would be useful, such as by the laser-induced-plasma ion-source-ion-trap technique of Fang and Kwong [11], but the experimental uncertainties [ $(\pm 0.2 - 0.3) \times 10^{-9} \text{ cm}^3 \text{ s}^{-1}$ ] at the typical measurement temperature ( $\sim 4000$  K) may not be sufficient to resolve the  $\sim 0.4 \times 10^{-9} \text{ cm}^3 \text{ s}^{-1}$  difference between our calculation and that of Opradolce *et al.*

Figure 7 also presents the rate coefficients for charge transfer due to collisions of  $\text{Si}^{4+}$  with  ${}^3\text{He}$  obtained directly from the  ${}^3\text{He}$  cross section and by mass scaling the energy dependence of the  ${}^4\text{He}$  cross section. Both procedures give  ${}^3\text{He}$  rate coefficients that agree at high temperatures as expected since the  ${}^3\text{He}$  and  ${}^4\text{He}$  cross sections are almost iden-

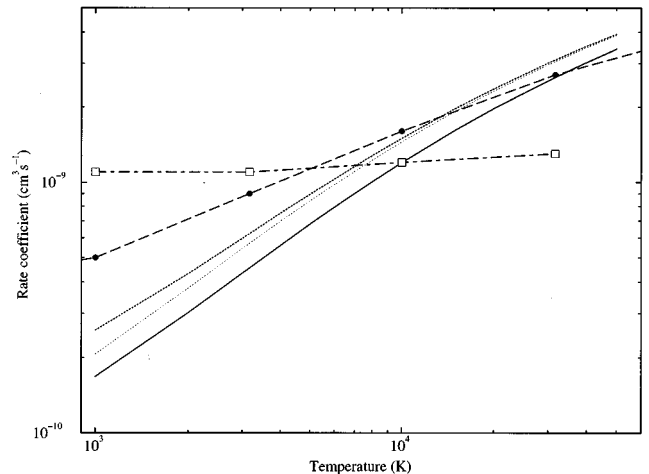


FIG. 7. Total electron capture rate coefficients. The designations are as given in Fig. 4 with the additions of  $\text{Si}^{4+} + {}^4\text{He}$ , Ref. [1] (dot-dashed line), and  $\text{Si}^{4+} + {}^3\text{He}$ , this work, determined with the  ${}^3\text{He}$  cross section (thick dotted line) and the mass-scaled  ${}^4\text{He}$  cross section (thin dotted line).

tical at high collision velocities, but at  $T=1000$  K the rate coefficient using the  $^3\text{He}$  cross section is 20% larger.

#### IV. ASTROPHYSICAL APPLICATIONS

The importance of charge transfer in astrophysical, as well as fusion, plasmas has been reviewed many times in the literature [12,13]. We restrict the discussion below to possible direct applications of reaction (1) in astrophysical environments. The Si IV  $3p\text{-}3s$  1400-Å line is observed in many types of gaseous nebulae and its intensity is routinely larger than predicted by photoionization models. For example, in the cataclysmic variable DQ Herculis [14], the 1400 Å line is  $\sim 2$  times larger than given by the appropriate x-ray illuminated nebula models of Kallman and McCray [15]. The models in Ref. [15] did not include charge transfer as a mechanism for populating the  $\text{Si}^{3+}(3p)$  level. To test the possible importance of charge transfer in such environments, the rate coefficients for reaction (1) as well as charge-transfer rate coefficients for collisions of  $\text{Si}^{4+}$  with H adapted from Gargaud and McCarroll [16] were provided to Kallman. He reran the photoionization model for a quasar emission line cloud with parameters similar to those chosen by Kwan and Krolik [17]. However, the model predicted that charge transfer would contribute only  $\sim 0.1\%$  to the total 1400-Å line intensity [18]. This can mostly be attributed to the very poor spatial overlap of  $\text{Si}^{4+}$  with neutral H and He in the cloud, which can be seen by examining the Si ionization structure for many of the models in Ref. [15]. Reaction (1), though, may play a role for x-ray sources embedded in diffuse or dense interstellar clouds.

The Si IV 1400-Å line is also observed in planetary nebulae [19] and astrophysical shocks [20]. Both Refs. [19] and [20] modeled these environments using the charge-transfer rate coefficients estimated by Butler and Dalgarno [1]. In planetary nebulae, the 1400-Å line is weak, difficult to ob-

serve, and may be attenuated by dust. Clegg *et al.* [19] modeled the 1400-Å line to be 9% smaller than observed, which does not confirm dust attenuation, and estimated the temperature of the  $\text{Si}^{4+}$  ions to be between  $\sim 14\,000$  and  $16\,500$  K. Our rate coefficients are  $\sim 30\%$  larger than those given in Ref. [1] in this temperature range and may therefore increase the modeled line intensity. Butler and Raymond [20] find that charge transfer decreases the  $\text{Si}^{4+}$  abundance for  $T \lesssim 25\,000$  K and increases the 1400-Å line intensity by 20% in a high-velocity shock. Our rate coefficients may also enhance these effects.

In the nebula of supernova ejecta, radioactive decay from  $^{56}\text{Co}$  heats and ionizes the gas. Through a variety of scattering and inner-shell transition processes energetic electrons are produced that collide with metals creating multiply charged ions. Charge exchange quickly drives the ionization stage of nearly all species to singly charged [21]. Reaction (1) may contribute significantly in such an environment.

#### V. CONCLUSION

We have presented a quantum-mechanical *ab initio* study of electron capture in collisions of  $\text{Si}^{4+}$  with He. The current results differ modestly from previous theoretical investigations. Low-energy measurements would be useful to discriminate between the various calculations. The process may be important in various astrophysical phenomena where a significant spatial overlap of  $\text{Si}^{4+}$  with neutral helium exists.

#### ACKNOWLEDGMENTS

We thank Dr. T. R. Kallman for helpful discussions and for testing the effects of charge transfer on photoionization models and the W. M. Keck Foundation for their generous support and funding of the W. M. Keck Laboratory for Computational Physics at UNLV. The work of P.C.S. and B.Z. is supported by NSF EPSCoR Grant No. OSR-9353227.

- 
- [1] S. E. Butler and A. Dalgarno, *Astrophys. J.* **241**, 838 (1980).  
 [2] L. Opradolce, R. McCarroll, and P. Valiron, *Astron. Astrophys.* **148**, 229 (1985).  
 [3] B. Zygelman, D. L. Cooper, M. J. Ford, A. Dalgarno, J. Gerratt, and M. Raimondi, *Phys. Rev. A* **46**, 3846 (1992).  
 [4] D. L. Cooper, J. Gerratt, and M. Raimondi, *Adv. Chem. Phys.* **69**, 319 (1987); *Int. Rev. Phys. Chem.* **7**, 59 (1988).  
 [5] N. J. Clarke, Doctoral thesis, University of Liverpool, 1995 (unpublished); N. J. Clarke, D. L. Cooper, J. Gerratt, and M. Raimondi (unpublished).  
 [6] S. Bashkin and J. O. Stoner, Jr., *Atomic Energy-Levels and Grottrian Diagrams* (North-Holland, Amsterdam, 1975).  
 [7] M. Oppenheimer, *J. Chem. Phys.* **57**, 3899 (1972).  
 [8] P. C. Stancil and B. Zygelman, *Phys. Rev. Lett.* **75**, 1495 (1995).  
 [9] R. E. Olson, *Phys. Rev. A* **2**, 121 (1970).  
 [10] S. D. Augustin, W. H. Miller, P. K. Pearson, and H. F. Schaefer III, *J. Chem. Phys.* **58**, 2845 (1973).  
 [11] Z. Fang and V. H. S. Kwong, *Phys. Rev. A* **51**, 1321 (1995).  
 [12] G. A. Shields, in *Molecular Astrophysics*, edited by T. W. Hartquist (Cambridge University Press, Cambridge, 1988), p. 461.  
 [13] P. C. Stancil, B. Zygelman, N. J. Clarke, and D. L. Cooper, *J. Phys. B* (to be published).  
 [14] A. D. Silber, S. F. Anderson, B. Margon, and R. A. Downes, *Astrophys. J.* **462**, 428 (1996).  
 [15] T. R. Kallman and R. McCray, *Astrophys. J. Suppl.* **50**, 263 (1982).  
 [16] M. Gargaud and R. McCarroll, *J. Phys. B* **21**, 513 (1988).  
 [17] J. Kwan and J. Krolik, *Astrophys. J.* **250**, 478 (1981).  
 [18] T. R. Kallman (private communication).  
 [19] R. E. S. Clegg, J. P. Harrington, M. J. Barlow, and J. R. Walsh, *Astrophys. J.* **314**, 551 (1987).  
 [20] S. E. Butler and J. C. Raymond, *Astrophys. J.* **240**, 680 (1980).  
 [21] S. Lepp, A. Dalgarno, and R. McCray, *Astrophys. J.* **358**, 262 (1990).